IEEE Photonics Journal
An IEEE Photonics Society Publication

Open Access

Integrated Optical Delay Line Based on a Loopback Arrayed Waveguide Grating for Radio-frequency Filtering

Volume 12, Number 3, June 2020

Xinyi Wang
Linjie Zhou
Liangjun Lu
Xingjun Wang
Jianping Chen

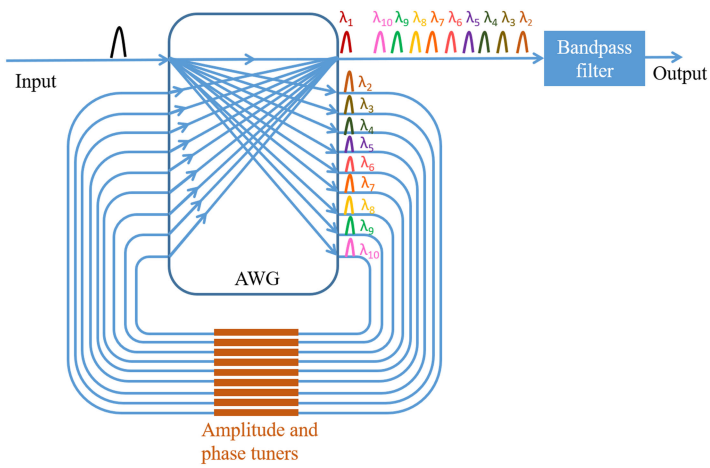

DOI: 10.1109/JPHOT.2020.2989431

Integrated Optical Delay Line Based on a Loopback Arrayed Waveguide Grating for Radio-frequency Filtering

Xinyi Wang,[1] **Linjie Zhou**,[1] **Liangjun Lu**,[1] **Xingjun Wang**,[2] **and Jianping Chen** [1]

[1]State key Laboratory of Advanced Optical Communication Systems and Networks, Department of Electronic Engineering, Shanghai Jiao Tong University, Shanghai 200240, China
[2]State Key Laboratory of Advanced Optical Communications System and Networks, School of Electronics Engineering and Computer Science, Peking University, Beijing, China

DOI:10.1109/JPHOT.2020.2989431

Manuscript received February 10, 2020; revised April 9, 2020; accepted April 18, 2020. Date of publication April 22, 2020; date of current version May 26, 2020. Corresponding author: Linjie Zhou (e-mail: ljzhou@sjtu.edu.cn).

Abstract: Integrated silicon photonics provides an attractive platform for on-chip radio-frequency (RF) signal processing. We demonstrate an integrated silicon optical delay line based on a loopback arrayed waveguide grating (AWG). The optical delay varies discretely by changing the carrier wavelength of the input optical signal. The device can be used as a multi-tap finite-impulse-response (FIR) radio-frequency filter, where each delay channel provides a feedforward replica of the RF signal. By changing the number of delay channels and the time interval between the channels, the bandwidth and center frequency of the RF filter can be tuned, respectively. The loopback AWG performs spectrum slicing and wavelength-selective delay, which greatly simplifies the light source requirement in FIR filter.

Index Terms: Waveguide devices, arrayed waveguide gratings, optical delay line, microwave photonics signal processing.

1. Introduction

Microwave photonics (MWP), which combines the radio-frequency (RF) engineering and the optoelectronics, has become a hot research field in recent years [1]–[4]. RF signals can be generated, transmitted and processed in the optical domain. A bunch of RF functions can be realized with the assistance of optical components to provide filtering, frequency multiplication/conversion [5], [6], arbitrary waveform generation [7], phase shifting, pulse shaping [8], and phased array beamforming [9], [10]. The ability of photonics in terms of wide bandwidth, parallelism, and adaptability has been well recognized.

The microwave photonic systems are becoming more complex in order to offer sophisticated functions. The systems composed of bulky components can no longer meet the requirements for light weight, small size, low power consumption, and long-term stability in practical usage. Integrated photonics provides a good solution. An integrated chip may contain multiple optical devices with high speed and a broad bandwidth [11]. A variety of photonic integration platforms are available for RF signal processing, including III-V semiconductors, silicon photonics, SiN/SiO_2 photonic integration, and hybrid integration of multiple materials. Due to the relatively large refractive

indices of silicon, silicon photonic integration features high compactness and small chip footprints. Moreover, electrical and optical components can be monolithically integrated into one chip using CMOS-compatible processes. It provides potential low-cost and mass production capabilities, which offers a key solution to reducing the cost of microwave photonic subsystems.

One of the enabling devices in microwave photonics is the optical delay line. It can be used for wideband signal processing, such as tunable high-resolution microwave filtering [12]–[16], beamforming in phased array antennas [17]–[21], and optical coherence tomography [22], [23]. Resonant devices including ring resonators [24]–[26], photonic crystal waveguides [27], [28], and Bragg gratings [29]–[31] can offer continuous delays. However, the performance is ultimately limited by the delay-bandwidth product, inherent to these resonant delay lines. Changing the physical length of the waveguide is another commonly used scheme to obtain a long delay. It is more straightforward and the achievable delay is proportional to the length of the waveguide [32]–[35]. In practice, the maximum achievable delay is only limited by the waveguide loss and the device size. The resolution of delay tuning is determined by the length difference of the waveguides. When an arrayed waveguide grating (AWG) is integrated with feedback waveguides with different lengths, the delay can be tuned by changing the carrier wavelength [36], [37].

Among the multiple MWP devices, a photonics-assisted RF filter is a basic component, which uses photonic devices to process RF signals [38]–[40]. RF photonic filters can be generally divided into three categories according to their implementation methods: RF-interference-based MWP filters [41]–[43], mapping the optical filter directly into the RF domain [44]–[46], and synthesis with multi-tap delay lines [47]–[49]. For the frequency mapping scheme, the filtering response is transferred from the optical domain to the RF domain and thus the filtering performance is basically limited by the optical filter. The implementation configuration is relatively simple. The RF-interference-based MWP filters rely on more complicated structures to get improved performances. Polarization-division-multiplexing Mach-Zehnder modulators and stimulated Brillouin scattering effects in optical fibers can be used to produce tunable RF filters with complementary bandpass and bandstop responses [50]. With the assist of two cascaded tunable Mach-Zehnder interferometers, the employment of under-coupled micro-ring resonators allows microwave photonic filters to possess narrow-band and ultra-high peak suppression capabilities [51]. Compared with these implementation methods, multi-tap RF filters are more flexible, in which the modulated optical signal is first replicated, then delayed with tailored amplitude, and finally summed together before detection by a photodetector to produce the RF output. It is essentially a finite-impulse-response (FIR)-type filter. Low-loss delay lines with large bandwidth are attractive for processing high-frequency RF signals. The high degree of flexibility in optical signal processing allows RF photonic filters to have several advantages over electronic counterparts, such as a highly programmable spectral shape and a fast-reconfigurable response. A single broadband light source (such as mode-locked laser [48] or c.w. incoherent light [52]) can be used in combination with a single dispersive element to implement a filter with multiple taps. RF filtering based on multi-tap delay lines is often implemented using optical fibers [49], [53]–[55].

Here, we present a multi-tap FIR RF filter based on a loopback AWG optical delay line on the silicon-on-insulator (SOI) platform. The key novelty of our scheme lies in the employment of an integrated loopback AWG both as a multi-wavelength filter and a dispersive element. Compared with other resonant dispersive devices, such as ring resonators, Bragg gratings, or photonic crystals, the loopback AWG gives a much larger dispersion and lower loss with a compact device footprint. Besides, owing to the spectrum slicing capability of the loopback AWG, our scheme only needs a broadband incoherent light source rather than a multi-wavelength laser array to obtain the filter taps. It thus greatly reduces the system complexity and cost.

The paper is organized as follows. Section 1 introduces the research background. In part 2.1 of section 2, we describe the structure and working principle of the loopback AWG. In part 2.2, we show the simulated performance of the device in response to a broadband input pulse in both time and frequency domains. In part 2.3, we characterize a single regular AWG. In part 2.4, we characterize a loopback AWG with the incremental delay being 10 ps. Section 3 demonstrates the multi-tap FIR RF filter based on the loopback AWG. Finally, Section 4 summarizes our work.

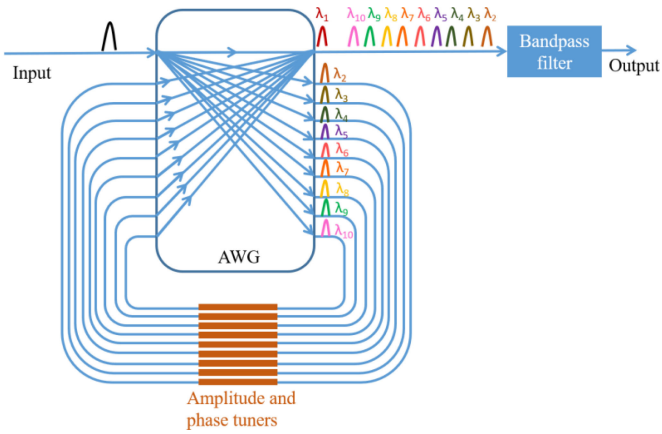

Fig. 1. Schematic structure of the loopback AWG.

2. Integrated Loopback AWG Optical Delay Line

2.1 Structure and Working Principle

Fig. 1(a) shows the structure of a 10 $\times$ 10 integrated loopback AWG. It has one open input-output pair and the other nine input-output pairs are connected by feedback waveguides. The incremental length of these feedback waveguides is constant, corresponding to a time step of *T*. This loopback AWG is topologically equivalent to two AWGs connected in series with delay waveguides in the middle. By reusing the same AWG as the wavelength multiplexer and de-multiplexer, the device footprint can be reduced by approximately a half. The channel wavelengths of the multiplexer and de-multiplexer are strictly aligned since they are from the same AWG.

Assuming a broadband optical pulse is launched into the input port of the loopback AWG, it is then sliced into 10 channels (λ_1 to λ_{10}) and spatially separated. The first wavelength λ_1 goes through to the output port, while the other nine wavelengths λ_2 to λ_{10} return to the input end of the AWG through the feedback waveguides. Due to the symmetry of the AWG, they recombine after certain delays with the first transmitted wavelength λ_1 at the output port. Since the length of the feedback waveguides increases linearly, the nine output pulses (λ_2 to λ_{10}) are evenly sequenced in the time domain. Therefore, the device can be used as a tunable optical delay line, with the delay amount dependent on its carrier wavelength. The delay can be tuned step by step by changing the carrier wavelength. The number of delays and resolution are decided by the port count of the AWG and the incremental length of the feedback waveguides, respectively. The envelope of the pulse sequence can be manipulated by varying the transmittivity of the feedback waveguides. In fact, by precisely controlling the amplitude and phase of each frequency component with a progressive Fourier synthesis method [36], [56], [57], optical arbitrary waveforms can be generated.

2.2 Device Simulation

Fig. 2 shows the simulation results of the loopback AWG by using Optisystem. The input is a Gaussian pulse (black line) generated by the optical Gaussian pulse generator with a width of 0.16 ps and a carrier wavelength of 1550 nm. The channel spacing is 200 GHz. An AWG with a smaller channel spacing leads to a larger footprint and deteriorated performance due to the increased inter-channel crosstalk. The channel bandwidth is 130 GHz. Nine pairs of input and output ports of the 10 $\times$ 10 AWG are connected with a gradually increasing delay of 10 ps as shown in Fig. 1. Optical spectrum analyzers and optical time-domain visualizers are used to detect the spectrum and time domain waveforms, respectively. After the input pulse passes the loopback AWG, multiple peaks appear on the spectrum (red line), as shown in Fig. 2(a). The wavelength channel (λ_1) passing the AWG once has a larger bandwidth than the other wavelength channels

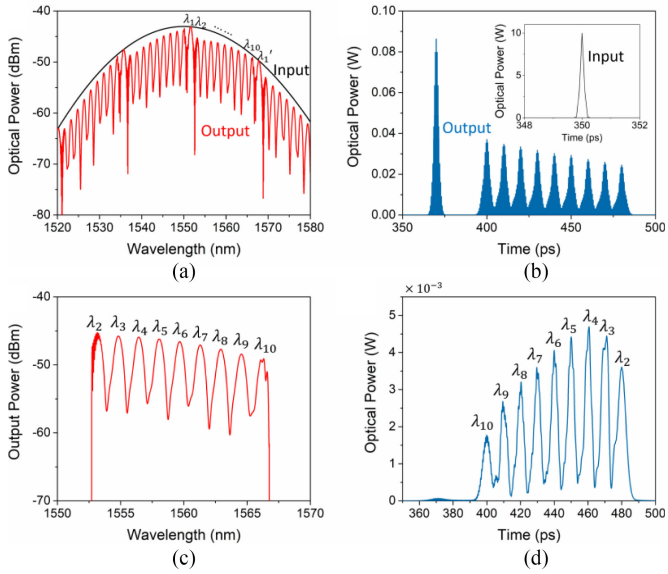

Fig. 2. (a) Simulated input (black) and output (red) optical spectra. (b) Waveform of the output pulse sequence. The inset shows the input single pulse. (c) Output optical spectrum after bandpass filtering. (d) Waveform of the filtered output pulse sequence.

(λ_2 to λ_{10}) that pass twice. The waveguide propagation loss is assumed to be 3 dB/cm, which is consistent with our practical device. Channels with relatively larger delays suffer higher losses.

The FSR of the AWG is determined by the incremental length ΔL of the arrayed waveguides in the AWG and expressed as $\lambda^2/(n_g \cdot \Delta L)$, where n_g is the group refractive index of the waveguide and λ is the free-space operation wavelength. If the bandwidth of the input pulse covers multiple FSRs of the AWG, then due to the recycling property of AWG, several wavelengths may reach the same destination port, such as λ_1 and λ_1' in Fig. 2(a).

The output pulse sequence has one strong leading pulse followed by nine low-amplitude pulses as shown in Fig. 2(b). The time interval of the latter nine pulses is 10 ps, governed by the delay step of the feedback waveguides. The pulse sequence can be further compressed (stretched) by transmission through a waveguide with negative (positive) dispersion. If the input pulse covers several FSRs of AWG, each output pulse would contain multiple carriers. We use an optical bandpass filter to eliminate the first pulse and limit the wavelength range within one FSR to avoid undesired interference of multiple carrier wavelengths. Figs. 2(c) and 2(d) show the filtered spectrum and the corresponding pulse sequence waveform, respectively. The filter has a 3-dB passband from 1552.71 nm to 1566.75 nm so that only 9 wavelengths (λ_2 to λ_{10}) are allowed to pass through.

2.3 Characterization of a Regular AWG

The AWG was fabricated on an SOI wafer with a top silicon layer thickness of 220 nm. In order to reduce the loss at the interface between the waveguides and the free propagation region (FPR), we used a three-layer taper to adiabatically expand the optical mode field. The width of the curved section of the waveguide is set to 450 nm to avoid excitation of higher-order modes. Straight waveguides are used for long-distance transmission and the width is widened to 800 nm to reduce light propagation loss. The narrow and wide waveguides are connected by a linear taper with a length of 20 μm. Fig. 3(a) shows the mask layout of the AWG. The length of the free propagation region (FPR) is 120 μm. The number of arrayed waveguides is 39 and the diffraction order is 80. The pitches of the input/output waveguides and the arrayed waveguides at the interface

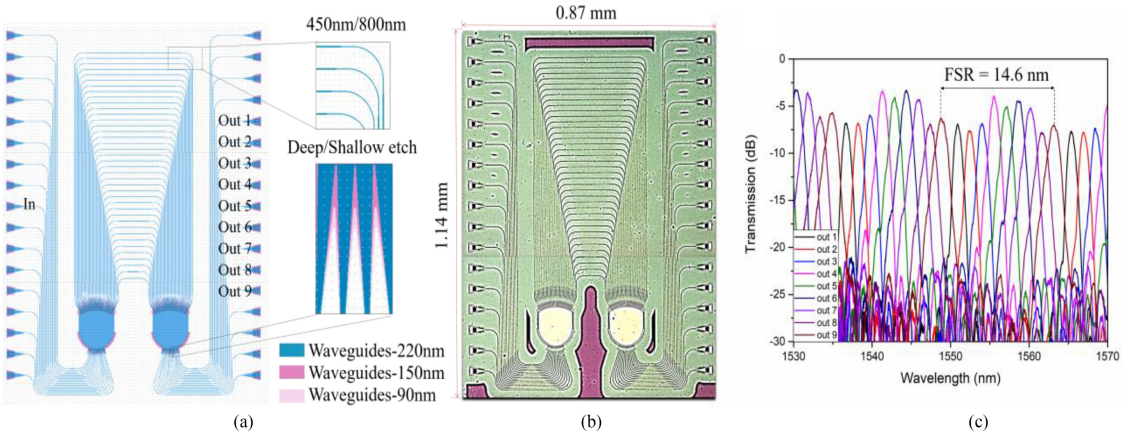

Fig. 3. (a) Mask layout of the single AWG. (b) Photograph of the fabricated device. (c) Measured transmission spectra of the single AWG normalized to a straight reference waveguide.

of the FPR are 3 μm and 2.42 μm, respectively. The device was simulated and optimized by using Lumerical finite-difference time-domain (FDTD) software. The arrayed waveguides have an incremental length difference of 45.16 μm, corresponding to an FSR of 14.4 nm. The FSR can incorporate 9 wavelength channels with a channel spacing of 200 GHz. Fig. 3(b) depicts the microscope image of the fabricated device. The device footprint is 1.14 mm $\times$ 0.87 mm. Fig. 3(c) presents the measured AWG spectrum by the loss and dispersion analyzer (Agilent, 86038B). Only the central nine output ports are selected in order to avoid spectral aliasing. The inter-channel crosstalk is lower than -15 dB. The crosstalk is mainly due to the phase errors in the arrayed waveguides. With better phase control in the arrayed waveguides by active (e.g., thermo-optic phase shifter) or passive (post-fabrication trimming) methods, the crosstalk can be suppressed and power transmission uniformity among channels can also be improved. The measured FSR is about 14.6 nm, slightly larger than the design. The channel spacing is around 200 GHz.

2.4 Characterization of a Loopback AWG

Figs. 4(a) and 4(b) show the mask layout and microscope image of the loopback AWG, respectively. The AWG design is the same as the previous regular AWG. Ten input/output ports in the center of the FPR are used. Fig. 4(c) illustrates the output spectrum of the loopback AWG. Similar to the single AWG, about 9 peaks are observed within one FSR of about 14.9 nm. Here the wavelength λ_{10} is obscured because the FSR is smaller than $10\Delta\lambda$. The total insertion loss of the device is approximately 16 dB, including 12 dB coupling loss owing to the unoptimized grating couplers. It is worth noting that the dense interference fringes inside the peaks come from the crosstalk between the AWG channels.

We used the first wavelength λ_1 as a reference to measure the amount of delay for the other wavelength channels. The first wavelength λ_1 passes the AWG only once, while the other wavelengths (λ_2 to λ_9) pass the AWG twice plus the feedback waveguides. Fig. 5 shows the delay of the nine channels, obtained by measuring the relative temporal position of the corresponding output optical pulses. In the measurement, an optical pulse obtained by modulating the laser light was used as input to the AWG. The relative delay of the output pulse when the laser wavelength was adjusted from λ_1 to λ_9 was recorded. The channels λ_2 to λ_9 have a 10-ps delay interval with a delay variance of 0.89 ps.

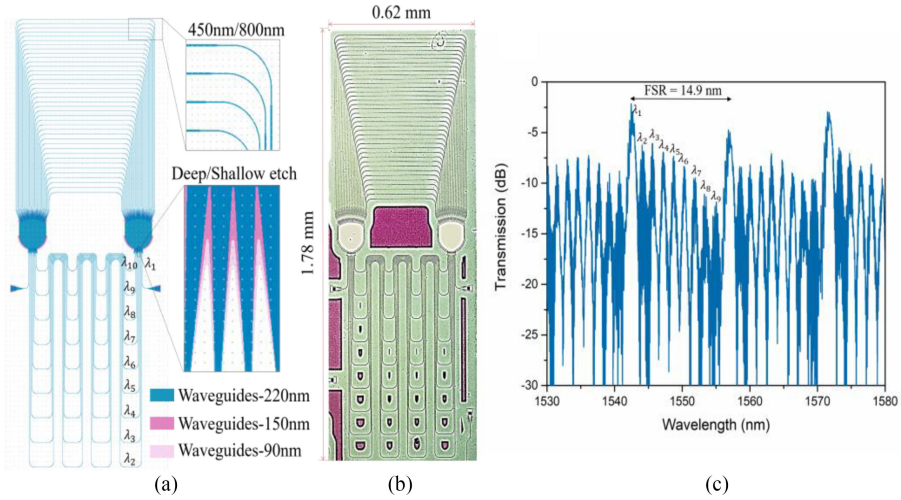

Fig. 4. (a) Mask layout of the loopback AWG. (b) Photograph of the fabricated device. (c) Measured transmission spectrum of the loopback AWG normalized to a straight reference waveguide.

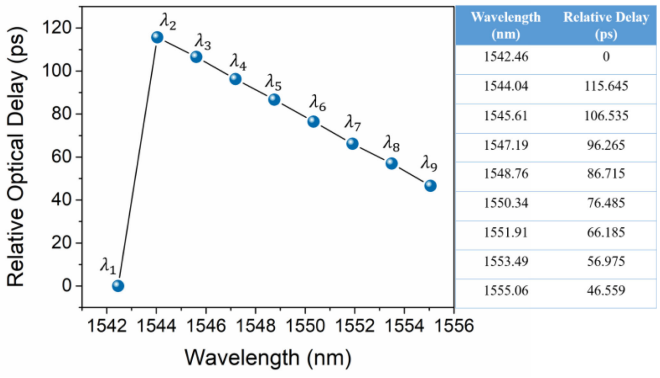

Wavelength (nm)	Relative Delay (ps)
1542.46	0
1544.04	115.645
1545.61	106.535
1547.19	96.265
1548.76	86.715
1550.34	76.485
1551.91	66.185
1553.49	56.975
1555.06	46.559

Fig. 5. Measured relative time delays from nice wavelength channels of the loopback AWG.

3. RF Filtering Based on the Loopback AWG

Low-loss broadband optical delay lines are attractive for processing high-frequency RF signals. In this section, we demonstrate that our loopback AWG-based delay line can be used to build an RF filter. Fig. 6 shows the working principle and the experimental setup. Light from a broadband supercontinuum source (YSL Photonics, sc-5-FC) is first intensity-modulated by the RF signal. The wavelength channels of the loopback AWG represent the taps of the FIR filter. Light going through the loopback AWG generates a group of weighted and delayed copies of the modulated optical signals. The number of delay channels is selected by the optical bandpass filter after the chip.

For our current device, the pulse delay interval is small (10 ps), mainly limited by the waveguide loss. This results in a large FSR in the RF spectrum. To reduce the FSR and set the center frequency of the RF filter to the measurable range of our equipment, we use a single-mode fiber as an additional dispersive element to increase the delay interval. It should be noted that the fiber is unnecessary if the loopback AWG were designed to have a larger delay interval of $>$100 ps. The employment of low-loss ultra-thin silicon waveguides [58] can greatly reduce the transmission loss

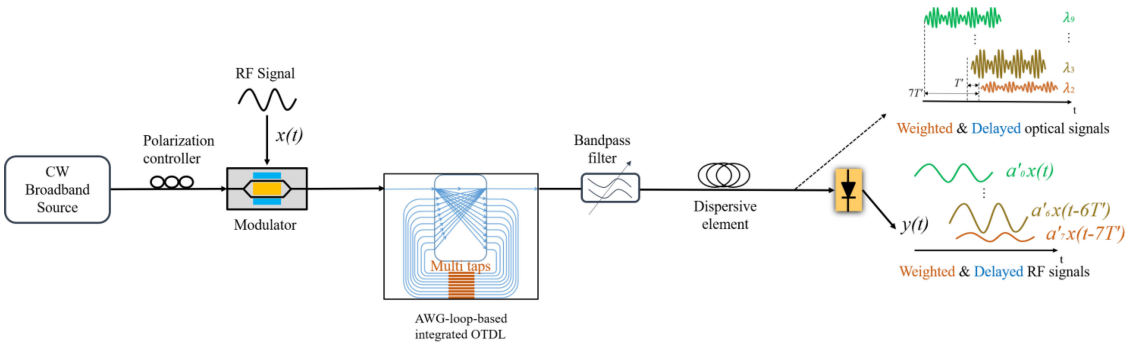

Fig. 6. Experimental setup for RF filter implementation using the loopback AWG.

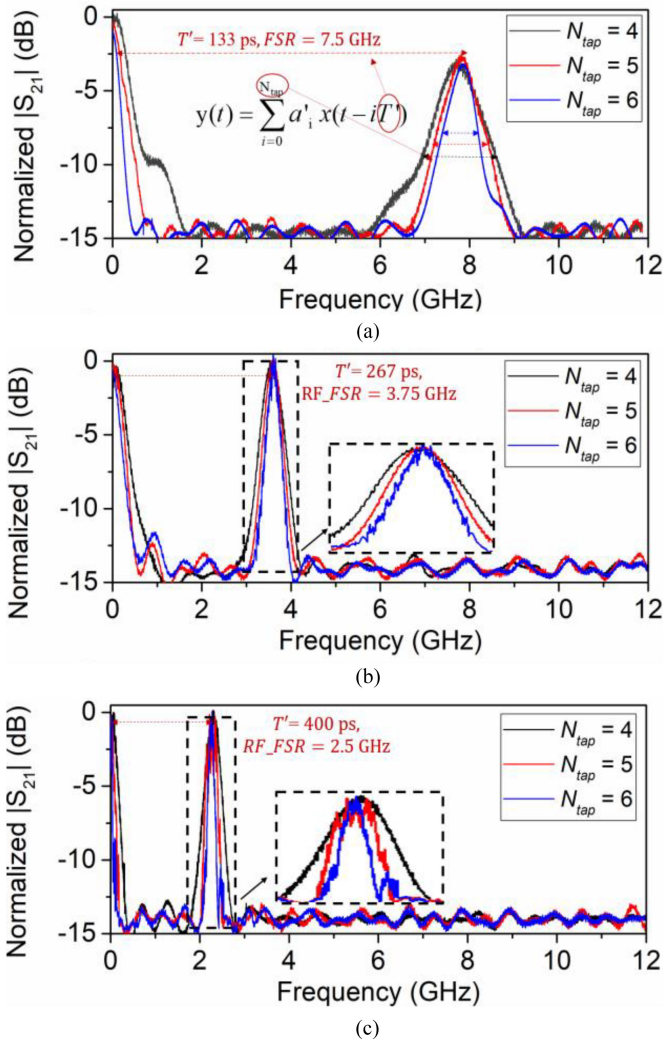

Fig. 7. Measured RF transfer functions when the time interval of the FIR filter is set to be (a) 133 ps, (b) 267 ps, and (c) 400 ps. In each plot, the filter tap N_{tap} varies from 4 to 6.

TABLE 1
Performance Comparison of Various Integrated RF Photonic Filters

Implementation method	Key device	Bandwidth (MHz)	Tuning Range (GHz)	Light source
Multi-tap synthesis	Silicon loopback AWG (this work)	220	2.5-7.5	A broadband light source
	SiN microring resonator [69]	1100	2.5-17.5	A frequency comb
	III-V photonic crystal [68]	1000	10-30	Multiple continuous-wave lasers
	Silicon microring resonator [67]	10	19.5-20.5	Multiple continuous-wave lasers
	Silicon microring resonator [14]	10	1.2-2.2	Multiple continuous-wave lasers
RF-interference	Silicon MZI and microring resonator [51]	780	0-40	A single continuous-wave laser
	SiN microring resonator [66]	247–850	2–15	A single continuous-wave laser
Frequency mapping	Silicon microring resonator [65]	6000	2.5-17.5	A single continuous-wave laser

of the waveguide. The transfer function of the system can then be expressed as:

$$y(t) = \sum_{i=0}^{N_{tap}} a_i' \, x(t - iT') \tag{1}$$

where $x(t)$ and $y(t)$ are the input and output RF signals in the time domain, respectively, N_{tap} is the number of taps, a_i' is the weight of each tap, and T' is the time delay between successive copies of modulated signals. The time delay is given by:

$$T' = D \cdot \Delta\lambda \cdot L + T \tag{2}$$

where D is the dispersion coefficient of the fiber, $\Delta\lambda$ is the channel spacing, L is the fiber length, and T is the delay interval of the loopback AWG. In our device, we have $D = 15.4$ ps/(nm.km), $\Delta\lambda = 1.6$ nm, and $T = 10$ ps.

Fig. 7(a) shows the electrical spectrum of the RF filter when L is chosen as 5 km. The time delay T' is about 133 ps and the corresponding center frequency of the RF passband is 7.5 GHz. Figs. 7(b) and 7(c) show the electrical spectra when the fiber is lengthened to give a longer time delay of 267 ps and 400 ps, respectively. As a result, the center frequency of the RF filter shifts to 3.75 GHz and 2.5 GHz. It should be noted that the RF spectrum has only one single passband except for the DC baseband. This is resulted from the sinusoidal and continuous optical tap weight distribution, as also observed and analyzed in other works [59], [60]. A DC block can be used after the filter to remove the baseband. It should be noted that a FIR filter designed with bipolar (both positive and negative) tap coefficients can suppress the baseband [54], [61]. The RF filter center frequency tuning range is 2.5–7.5 GHz, larger than all-electronic filters [62], [63]. It can be further expanded by adjusting the length of the fiber. Besides the center frequency, we can also control the bandwidth of the RF passband. In Fig. 7(a), when four wavelength channels (λ_4 to λ_7) are selected ($N_{tap} = 4$) by the optical bandpass filter, the 3-dB bandwidth (BW) of the RF passband is 0.98 GHz. When the channel number is increased to $N_{tap} = 5$ and 6, the RF bandwidth is reduced to 0.81 GHz and 0.67 GHz, respectively. In fact, amplitude and phase tuners can be integrated in the feedback waveguides as schematically shown in Fig. 1, and in this way it can offer a greater flexibility as each tap coefficient can be independently tuned. The RF bandwidth and the number of taps are roughly inversely proportional. Compared to other integrated RF photonic filters [51], [64]–[66], our RF filter can achieve a narrower bandwidth, as shown in Table 1. The smallest bandwidth of the 6-tap filter in Fig. 7(c) is about 220 MHz. For multi-tap delay lines, our solution only requires a

broadband incoherent light source instead of expensive multi-wavelength laser arrays [14], [67], [68] or frequency combs [69].

4. Conclusion

We have demonstrated a compact integrated silicon optical delay line based on a spectrally-cyclic loopback AWG. The delay of the output signal can be tuned by changing the signal carrier wavelength. The delay tuning resolution is 10 ps and 9 delay tuning steps are obtained. As a proof-of-principle application of the device, we implemented a multi-tap FIR RF filter based on the loopback AWG. The RF filter is tunable in both the center frequency and the bandwidth. The center frequency can be changed by varying the dispersive fiber length after the device. The filter bandwidth can be changed by selecting the number of delay channels. Thanks to the high integration capability of silicon photonics, all discrete components (like modulator, filter, PD, etc.) can potentially be integrated with the loopback AWG on a single chip, making it possible to realize a monolithically integrated RF filter.

References

[1] J. Capmany and D. Novak, "Microwave photonics combines two worlds," *Nature Photon., Rev. Article*, vol. 1, p. 319, 2007.
[2] L. R. Chen, "Silicon photonics for microwave photonics applications," *J. Lightw. Technol.*, vol. 35, no. 4, pp. 824–835, 2017.
[3] W. Zhang and J. Yao, "Silicon-based integrated microwave photonics," *IEEE J. Quantum Electron.*, vol. 52, no. 1, pp. 1–12, 2016.
[4] D. Marpaung, J. Yao, and J. Capmany, "Integrated microwave photonics," *Nature Photon.*, vol. 13, no. 2, pp. 80–90, 2019.
[5] Y. Zhong *et al.*, "Microwave frequency upconversion employing a coupling-modulated ring resonator," *Photon. Res.*, vol. 5, no. 6, pp. 689–694, 2017.
[6] Y. Long, L. Zhou, and J. Wang, "Photonic-assisted microwave signal multiplication and modulation using a silicon Mach–Zehnder modulator," *Scientific Rep., Article*, vol. 6, 2016, Art. no. 20215.
[7] X. Wang *et al.*, "Continuously tunable ultra-thin silicon waveguide optical delay line," *Optica*, vol. 4, no. 5, pp. 507–515, 2017.
[8] J. Xie, L. Zhou, Z. Li, J. Wang, and J. Chen, "Seven-bit reconfigurable optical true time delay line based on silicon integration," *Opt. Express*, vol. 22, no. 19, pp. 22707–22715, 2014.
[9] T. Tatoli, D. Conteduca, F. Dell'Olio, C. Ciminelli, and M. N. Armenise, "Graphene-based fine-tunable optical delay line for optical beamforming in phased-array antennas," *Appl. Opt.*, vol. 55, no. 16, pp. 4342–4349, 2016.
[10] G. Hu *et al.*, "Optical beamformer based on diffraction order multiplexing (DOM) of an arrayed waveguide grating," *J. Lightw. Technol.*, pp. 1–1, 2019.
[11] L. Lu *et al.*, "16 $\times$ 16 non-blocking silicon optical switch based on electro-optic Mach-Zehnder interferometers," *Opt. Express*, vol. 24, no. 9, pp. 9295–9307, 2016.
[12] V. Polo, B. Vidal, J. L. Corral, and J. Marti, "Novel tunable photonic microwave filter based on laser arrays and N/spl times/N AWG-based delay lines," *IEEE Photon. Technol. Lett.*, vol. 15, no. 4, pp. 584–586, 2003.
[13] A. Mokhtari, K. Jamshidi, S. Preußler, A. Zadok, and T. Schneider, "Tunable microwave-photonic filter using frequency-to-time mapping-based delay lines," *Opt. Express*, vol. 21, no. 18, pp. 21702–21707, 2013.
[14] M. Burla *et al.*, "On-chip CMOS compatible reconfigurable optical delay line with separate carrier tuning for microwave photonic signal processing," *Opt. Express*, vol. 19, no. 22, pp. 21475–21484, 2011.
[15] S. Chin *et al.*, "Broadband true time delay for microwave signal processing, using slow light based on stimulated Brillouin scattering in optical fibers," *Opt. Express*, vol. 18, no. 21, pp. 22599–22613, 2010.
[16] I. Aryanfar *et al.*, "Chip-based Brillouin radio frequency photonic phase shifter and wideband time delay," *Opt. Lett.*, vol. 42, no. 7, pp. 1313–1316, 2017.
[17] J. Yao, "Microwave photonics," *J. Lightw. Technol.*, vol. 27, no. 3, pp. 314–335, 2009.
[18] Y. Liu *et al.*, "Ultra-low-loss silicon nitride optical beamforming network for wideband wireless applications," *IEEE J. Sel. Topics Quantum Electron.*, vol. 24, no. 4, pp. 1–10, 2018.
[19] W. Zhou *et al.*, "Developing an integrated photonic system with a simple beamforming architecture for phased-array antennas," *Appl. Opt.*, vol. 56, no. 3, pp. B5–B13, 2017.
[20] L. Zhuang *et al.*, "Novel ring resonator-based integrated photonic beamformer for broadband phased array receive antennas—Part II: Experimental prototype," *J. Lightw. Technol.*, vol. 28, no. 1, pp. 19–31, 2010.
[21] M. A. Piqueras *et al.*, "Optically beamformed beam-switched adaptive antennas for fixed and mobile broad-band wireless access networks," *IEEE Trans. Microw. Theory Techn.*, vol. 54, no. 2, pp. 887–899, 2006.
[22] M. G. Hyeon, H.-J. Kim, B.-M. Kim, and T. J. Eom, "Spectral domain optical coherence tomography with balanced detection using single line-scan camera and optical delay line," *Opt. Express*, vol. 23, no. 18, pp. 23079–23091, 2015.
[23] K. Takiguchi, M. Itoh, and H. Takahashi, "Integrated-optic variable delay line and its application to a low-coherence reflectometer," *Opt. Lett.*, vol. 30, no. 20, pp. 2739–2741, 2005.

[24] J. Yang *et al.*, "Continuously tunable, wavelength-selective buffering in optical packet switching networks," *IEEE Photon. Technol. Lett.*, vol. 20, no. 12, pp. 1030–1032, 2008.
[25] N. Fontaine *et al.*, "Continuously tunable optical buffering at 40 gb/s for optical packet switching networks," *J. Lightw. Technol.*, vol. 26, no. 23, pp. 3776–3783, 2008.
[26] D. Conteduca, F. Dell'Olio, C. Ciminelli, and M. N. Armenise, "Resonant graphene-based tunable optical delay line," *IEEE Photon. J.*, vol. 7, no. 6, 2015, Art. no. 7802409.
[27] Y. A. Vlasov, M. O'Boyle, H. F. Hamann, and S. J. McNab, "Active control of slow light on a chip with photonic crystal waveguides," *Nature*, vol. 438, p. 65, 2005.
[28] J. Sancho *et al.*, "Integrable microwave filter based on a photonic crystal delay line," *Nature Commun.*, vol. 3, p. 1075, 2012.
[29] I. Giuntoni *et al.*, "Continuously tunable delay line based on SOI tapered Bragg gratings," *Opt. Express*, vol. 20, no. 10, pp. 11241–11246, 2012.
[30] G. Brunetti, D. Conteduca, F. Dell'Olio, C. Ciminelli, and M. N. Armenise, "Design of an ultra-compact graphene-based integrated microphotonic tunable delay line," *Opt. Express*, vol. 26, no. 4, pp. 4593–4604, 2018.
[31] X. Wang, Y. Zhao, Y. Ding, S. Xiao, and J. Dong, "Tunable optical delay line based on integrated grating-assisted contradirectional couplers," *Photon. Res.*, vol. 6, no. 9, pp. 880–886, 2018.
[32] X. Wang, B. Howley, M. Y. Chen, and R. T. Chen, "Phase error corrected 4-bit true time delay module using a cascaded 2×2 polymer waveguide switch array," *Appl. Opt.*, vol. 46, no. 3, pp. 379–383, 2007.
[33] J. Wang *et al.*, "Subwavelength grating enabled on-chip ultra-compact optical true time delay line," *Scientific Rep.*, vol. 6, 2016, Art. no. 30235.
[34] M. S. Rasras *et al.*, "Integrated resonance-enhanced variable optical delay lines," *IEEE Photon. Technol. Lett.*, vol. 17, no. 4, pp. 834–836, 2005.
[35] Q. Q. Song, Z. F. Hu, and K. X. Chen, "Scalable and reconfigurable true time delay line based on an ultra-low-loss silica waveguide," *Appl. Opt.*, vol. 57, no. 16, pp. 4434–4439, 2018.
[36] N. K. Fontaine *et al.*, "Compact 10 GHz loopback arrayed-waveguide grating for high-fidelity optical arbitrary waveform generation," *Opt. Lett.*, vol. 33, no. 15, pp. 1714–1716, 2008.
[37] Z. Cao *et al.*, "Integrated remotely tunable optical delay line for millimeter-wave beam steering fabricated in an InP generic foundry," *Opt. Lett.*, vol. 40, no. 17, pp. 3930–3933, 2015.
[38] J. Capmany, J. Mora, I. Gasulla, J. Sancho, J. Lloret, and S. Sales, "Microwave photonic signal processing," *J. Lightw. Technol.*, vol. 31, no. 4, pp. 571–586, 2013.
[39] J. Capmany, B. Ortega, and D. Pastor, "A tutorial on microwave photonic filters," *J. Lightw. Technol.*, vol. 24, no. 1, pp. 201–229, 2006.
[40] R. A. Minasian, "Photonic signal processing of microwave signals," *IEEE Trans. Microw. Theory Techn.*, vol. 54, no. 2, pp. 832–846, 2006.
[41] W. Zhang and R. A. Minasian, "Switchable and tunable microwave photonic brillouin-based filter," *IEEE Photon. J.*, vol. 4, no. 5, 2012.
[42] D. Marpaung *et al.*, "Low-power, chip-based stimulated Brillouin scattering microwave photonic filter with ultrahigh selectivity," *Optica*, vol. 2, no. 2, pp. 76–83, 2015.
[43] Y. Liu, J. Hotten, A. Choudhary, B. J. Eggleton, and D. Marpaung, "All-optimized integrated RF photonic notch filter," *Opt. Lett.*, vol. 42, no. 22, pp. 4631–4634, 2017.
[44] J. Palaci, G. E. Villanueva, J. V. Galan, J. Marti, and B. Vidal, "Single bandpass photonic microwave filter based on a notch ring resonator," *IEEE Photon. Technol. Lett.*, vol. 22, no. 17, pp. 1276–1278, 2010.
[45] J. Palaci *et al.*, "Tunable photonic microwave filter with single bandpass based on a phase-shifted fiber bragg grating," *IEEE Photon. Technol. Lett.*, vol. 22, no. 19, pp. 1467–1469, 2010.
[46] Y. Deng, M. Li, J. Tang, S. Sun, N. Huang, and N. Zhu, "Widely tunable single-passband microwave photonic filter based on DFB-SOA-assisted optical carrier recovery," *IEEE Photon. J.*, vol. 7, no. 5, 2015, Art. no. 5501108.
[47] J. Capmany, D. Pastor, and B. Ortega, "New and flexible fiber-optic delay-line filters using chirped Bragg gratings and laser arrays," *IEEE Trans. Microw. Theory Techn.*, vol. 47, no. 7, pp. 1321–1326, 1999.
[48] A. Ortigosa-Blanch, J. Mora, J. Capmany, B. Ortega, and D. Pastor, "Tunable radio-frequency photonic filter based on an actively mode-locked fiber laser," *Opt. Lett.*, vol. 31, no. 6, pp. 709–711, 2006.
[49] X. Xue, X. Zheng, H. Zhang, and B. Zhou, "Highly reconfigurable microwave photonic single-bandpass filter with complex continuous-time impulse responses," *Opt. Express*, vol. 20, no. 24, pp. 26929–26934, 2012.
[50] P. Li, W. Pan, X. Zou, L. Yan, and Y. Pan, "Tunable photonic radiofrequency filter with complementary bandpass and bandstop responses," *Opt. Lett.*, vol. 42, no. 16, pp. 3129–3132, 2017.
[51] X. Liu, Y. Yu, H. Tang, L. Xu, J. Dong, and X. Zhang, "Silicon-on-insulator-based microwave photonic filter with narrowband and ultrahigh peak rejection," *Opt. Lett.*, vol. 43, no. 6, pp. 1359–1362, 2018.
[52] J. H. Lee, Y. M. Chang, Y.-G. Han, S. B. Lee, and H. Y. Chung, "Fully reconfigurable photonic microwave transversal filter based on digital micromirror device and continuous-wave, incoherent supercontinuum source," *Appl. Opt.*, vol. 46, no. 22, pp. 5158–5167, 2007.
[53] V. R. Supradeepa *et al.*, "Comb-based radiofrequency photonic filters with rapid tunability and high selectivity," *Nature Photon.*, vol. 6, p. 186, 2012.
[54] L. Li, X. Yi, T. X. H. Huang, and R. A. Minasian, "Distortion-free spectrum sliced microwave photonic signal processor: analysis, design and implementation," *Opt. Express*, vol. 20, no. 10, pp. 11517–11528, 2012.
[55] E. H. W. Chan and R. A. Minasian, "Coherence-free high-resolution RF/microwave photonic bandpass filter with high skirt selectivity and high stopband attenuation," *J. Lightw. Technol.*, vol. 28, no. 11, pp. 1646–1651, 2010.
[56] N. K. Fontaine *et al.*, "32 phase$\times$32 amplitude optical arbitrary waveform generation," *Opt. Lett.*, vol. 32, no. 7, pp. 865–867, 2007.
[57] K. Takiguchi, T. Kominato, H. Takahashi, T. Shibata, and K. Okamoto, "Flexible pulse waveform generation using a silica waveguide based spectrum synthesis circuit," in *Proc. Opt. Fiber Commun. Conf.*, Los Angeles, CA, USA, 2004, Paper TuI5.

[58] Z. Zou, L. Zhou, X. Li, and J. Chen, "60-nm-thick basic photonic components and Bragg gratings on the silicon-on-insulator platform," *Opt. Express*, vol. 23, no. 16, pp. 20784–20795, 2015.
[59] J. Mora *et al.*, "Photonic microwave tunable single-bandpass filter based on a Mach-Zehnder interferometer," *J. Lightw. Technol.*, vol. 24, no. 7, p. 2500, 2006.
[60] J. Mora, L. R. Chen, and J. Capmany, "Single-bandpass microwave photonic filter with tuning and reconfiguration capabilities," *J. Lightw. Technol.*, vol. 26, no. 15, pp. 2663–2670, 2008.
[61] J. Capmany, D. Pastor, A. Martinez, B. Ortega, and S. Sales, "Microwave photonic filters with negative coefficients based on phase inversion in an electro-optic modulator," *Opt. Lett.*, vol. 28, no. 16, pp. 1415–1417, 2003.
[62] B. Kim, J. Lee, J. Lee, B. Jung, and W. J. Chappell, "RF CMOS integrated on-chip tunable absorptive bandstop filter using Q-tunable resonators," *IEEE Trans. Electron Devices*, vol. 60, no. 5, pp. 1730–1737, 2013.
[63] E. J. Naglich, A. C. Guyette, and D. Peroulis, "High-Q intrinsically-switched quasi-absorptive tunable bandstop filter with electrically-short resonators," in *Proc. IEEE MTT-S Int. Microw. Symp.*, 2014, pp. 1–4.
[64] M. S. Rasras *et al.*, "Demonstration of a tunable microwave-photonic notch filter using low-loss silicon ring resonators," *J. Lightw. Technol.*, vol. 27, no. 12, pp. 2105–2110, 2009.
[65] J. Dong *et al.*, "Compact notch microwave photonic filters using on-chip integrated microring resonators," *IEEE Photon. J.*, vol. 5, no. 2, 2013, Art. no. 5500307.
[66] D. Marpaung *et al.*, "Si3N4 ring resonator-based microwave photonic notch filter with an ultrahigh peak rejection," *Opt. Express*, vol. 21, no. 20, pp. 23286–23294, 2013.
[67] J. Lloret *et al.*, "Tunable complex-valued multi-tap microwave photonic filter based on single silicon-on-insulator microring resonator," *Opt. Express*, vol. 19, no. 13, pp. 12402–12407, 2011.
[68] J. Sancho *et al.*, "Integrable microwave filter based on a photonic crystal delay line," *Nature Commun.*, vol. 3, no. 1, p. 1075, 2012.
[69] X. Xue *et al.*, "Programmable single-bandpass photonic RF filter based on kerr comb from a microring," *J. Lightw. Technol.*, vol. 32, no. 20, pp. 3557–3565, 2014.